



Insights into spring-back prediction: a comparative analysis of constitutive models for perforated U-shaped roll-formed steel profiles

Saeid Hajiahmadi¹ · Hassan Moslemi Naeini^{1,2} · Hossein Talebi-Ghadikolae³ · Rasoul Safdarian⁴ · Ali Zeinolabedin-Beygi¹

Received: 25 February 2024 / Accepted: 25 July 2024 / Published online: 12 August 2024
© The Author(s), under exclusive licence to Springer-Verlag London Ltd., part of Springer Nature 2024

Abstract

This study aimed to investigate the influence of different constitutive models on the accuracy of predicting spring-back in cold roll forming for pre-punched profiles. Finite element analysis was conducted using Abaqus, employing eight distinct constitutive models that varied in terms of yield criteria, yield function calibration, and elastic modulus degradation. To evaluate the impact of holes and their positions on spring-back, three samples made of St12 with a 1 mm thickness were used: a sample without holes, a profile with holes in the bending zone (on the bend), and a profile with holes close to the bending zone (near the bend). The results show that ignoring variation in elastic modulus has less influence on the accuracy of spring-back prediction for “near the bend” than the two other profiles. This case is explained by less change in elastic modulus during roll forming of the “near the bend” profile. Additionally, calibrating yield criteria based on *R*-values, such as Hill48_R and Yld89_R, and yield stress values result in more precise spring-back estimations for the “on the bend” and “near the bend” profiles, respectively. This approach proves superior when contrasted with the alternative calibration methods. Moreover, neglecting the effect of Young’s modulus variation in Yld2000-2d and Hill48_S results in the lowest MAPE (mean absolute percentage error) of approximately 20% compared to other models. However, it is worth noting that Yld2000-2d underestimates the experimental values while Hill48_S tends to overestimate them. As a result, the most suitable constitutive model, considering elastic variation, is Yld2000-2d, with an average MAPE of 8% across all three samples.

Keywords Metal forming · Cold roll forming · Constitutive models · Spring-back · Elastic modulus variation

1 Introduction

Nowadays, forming processes have gained significant popularity for producing metal [1–3] and composite [4, 5] parts. Among these sheet metal forming techniques, processes

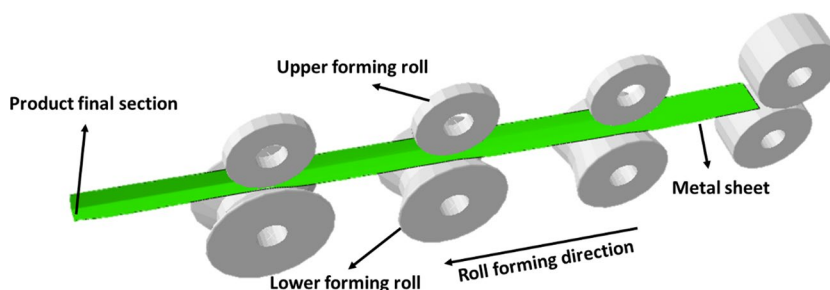
characterized by dominant bending deformation modes have received considerable attention [6, 7]. Cold roll forming, which relies on bending as its primary deformation mode, has become particularly prominent in industrial-scale production due to its capacity for mass production [8]. This method employs multiple forming stations, each equipped with at least two rollers, as shown in Fig. 1. These rollers guide the sheet metal through their gap, gradually bending it into the desired profile while the rollers rotate. The final profile shape is achieved as the sheet passes through different forming stations, culminating in the last station, where the desired profile’s final shape is attained [9].

The roll-forming process can be divided into two categories based on the final cross-section of the produced samples: conventional [10] and flexible roll forming [11]. The traditional roll-forming method can create samples with a consistent cross-sectional shape along their entire length. In contrast, a flexible roll-forming method has been

✉ Hassan Moslemi Naeini
moslemi@modares.ac.ir

¹ Materials Forming Laboratory, School of Mechanical Engineering, Tarbiat Modares University, Tehran, Islamic Republic of Iran
² Academic Center for Education, Culture and Research (ACECR), Tehran, Islamic Republic of Iran
³ Faculty of Mechanical Engineering, University of Kashan, Kashan, Islamic Republic of Iran
⁴ Department of Mechanical Engineering, Qom University of Technology, Qom, Islamic Republic of Iran

Fig. 1 Schematic diagram of roll-forming process



recently developed, enabling the production of long sections with varying widths and heights.

Cold rolled pre-punched profiles are common in industries like automotive, construction, and aerospace for structural applications. They require precise dimensional tolerances and accurate spring-back prediction to maintain high dimensional tolerances, which is related to the spring-back value. In fact, accurate prediction of spring-back is essential for maintaining tight dimensional tolerances, which are critical in applications where precise fit and alignment are required. Moreover, by improving the accuracy of spring-back predictions, manufacturers can reduce the need for costly and time-consuming trial-and-error adjustments during the tooling design and forming process. This leads to increased efficiency and cost savings. Finally, enhanced prediction accuracy contributes to higher quality control standards, minimizing defects and rework and ensuring consistent product quality.

Like other metal forming processes, roll forming is susceptible to various changes in the final profile contour due to phenomena such as bowing and twisting. Safdarian et al. [12] investigated the effect of bending angle on bowing, while Tajik et al. [13] focused on reducing twisting in asymmetrical channel sections. These studies provide valuable insights into contour changes during roll forming. Moreover, Talebi-Ghadikolaee et al. [14] addressed fracture prediction during the roll-forming process. While these contour changes are important considerations, spring-back presents a significant challenge in roll forming.

Spring-back is a significant concern in the roll-forming process, affecting the dimensional accuracy of final profiles. This phenomenon primarily occurs due to the release of elastic strain during unloading after plastic deformation. As the material undergoes plastic deformation, it accumulates elastic strain energy, which is released upon unloading, causing the material to return to its original shape. Factors such as material properties, process parameters, and tooling conditions can influence spring-back magnitude. Achieving an accurate spring-back prediction requires consideration of appropriate unloading behavior and the underlying mechanisms governing elastic recovery.

The amount of spring back observed after unloading (removal of the forming tools) is significantly influenced by the elastic stiffness of the material, i.e., its Young's modulus. In classic plasticity theory, the unloading following plastic deformation is assumed to be linearly elastic, with a stiffness equal to Young's modulus. However, numerous experimental studies have demonstrated that this assumption is not accurate. Evidence from Sumikawa [15], Kim [16], and Chatti and Hermi [17] has shown that as plastic strain accumulates during plastic work, the elastic stiffness of the material decreases. Subsequent studies by Yoshida et al. [18], Sun and Wagoner [19], and Chatti et al. [20] revealed that the stress–strain relationship during unloading exhibits a somewhat curved behavior rather than being linear. Yoshida et al. [21] proposed a model to consider this nonlinearity, but they concluded that the error incurred by ignoring it is relatively tiny in spring-back simulation.

The selection of the yield criterion in finite element simulations for predicting spring-back is paramount, as it defines a closed yield stress surface in space that bounds the range of elastic behavior of the material [22]. In their study, Lin et al. [23] highlighted that for materials like MP980, which exhibit an apparent Bauschinger effect but insignificant texture anisotropy, the choice of an appropriate yield criterion (e.g., Hill48), along with considering elastic modulus degradation combined with the Yoshida-Umeri hardening model, significantly enhances the accuracy of spring-back prediction. On the other hand, for materials such as AA6022-T4, which show little Bauschinger effect but have significant texture anisotropy, the use of a yield criterion that accounts for anisotropy (e.g., YLD2000-2D) becomes more crucial for improving the accuracy of spring-back prediction. Lee et al. [24], in their comparative study of spring-back prediction based on Von Mises and Yld2000-2d for isotropic DP780 materials, observed no noticeable difference in the results due to the isotropy of the material. Additionally, Seo et al. [25] concluded that using Barlat2000-2d instead of Hill's 48 is more accurate in cold stamping, primarily due to the complex deformation involved in the forming process.

Numerous scholars have extensively investigated the spring-back phenomena in cold roll forming (CRF). Liu et al. [26] demonstrated a remarkable 25% increase in the

accuracy of spring-back prediction for UHSS hat profiles in CRF when using the Yld2000-2d yield criterion compared to the Von Mises yield criterion. Naofal et al. [27] delved into the effect of variable elastic modulus and hardening models in predicting the spring-back of St37 profiles through FE modeling.

Despite the importance of spring-back prediction in roll forming for pre-punched profiles, this aspect remains largely unexplored in the existing research. Currently, no investigation specifically focuses on the effect of using different constitutive models on spring-back prediction obtained through numerical methods, nor any comparison to propose an accurate and reliable model for this matter. Bidabadi et al. [28, 29] studied the ovality of circular holes and bowing defects in the flange area of punched profiles. In their research, Farsi et al. [30] examined the spring-back of a sheet with an oval hole in the bend area, subjected to bending by a brake press, utilizing both experimental and FE (finite element) methods. Subsequently, Nasrollahi [30] extended this work. In the context of low-carbon steel, Nasrollahi's findings [30] indicated that maximum spring-back occurs when the hole percentage in the bending area length reaches about 40%. Nikhare et al. [31] reported that a higher material thickness increases spring-back when a material discontinuity is present at the bend line during the L-bending of AA5083. Interestingly, this finding contradicted the general trend predicted by conventional theories. Through experimental observations, Thipprakmas et al. [32] noted that the presence of holes in the bending zone increased spring-back to a greater extent than holes located near the bending zone during V-die bending of aluminum alloy AA1100.

The research aims to create a reliable model for accurately predicting plastic and elastic deformation behavior in profiles during the roll-forming process, focusing on spring-back phenomena in pre-punched profiles. The study employs various yield criteria and calibration methods to compare constitutive models and achieve precise spring-back prediction. Four criteria are used, including the Von Mises isotropic yield criterion and anisotropic Hill1948, Yld89, and Yld2000-2d yield criteria.

The study focuses on predicting spring-back behavior in industrial profiles using a hole-less sample, a profile with holes in the bending zone, and a profile with holes close to the bending zone. The hole-less sample serves as a baseline, while the profile with holes in the bending zone introduces stress concentration and alters material flow. The profile with holes close to the bending zone investigates the impact of hole position on deformation mode and model accuracy. These profiles represent common industrial scenarios where pre-punched holes are strategically placed to meet design and functional requirements. The presence and position of holes significantly alter the stress state and deformation mechanics during the forming process. Comparing

predictive accuracy across profiles helps identify the most robust and reliable models for practical applications, optimizing the roll-forming process and ensuring product quality and precision.

This study conducted uniaxial tensile, loading–unloading–reloading, and hydraulic bulge tests to calibrate constitutive models. Experimental roll forming was performed on three samples: without holes, holes in the bending zone, and adjacent to the bending zone. The profiles were incrementally bent by 15° to reach a 45° angle, with measurements taken at 15, 30, and 45° in every profile. Finite element simulations assessed spring-back prediction accuracy, comparing numerical predictions with actual measurements taken during the roll-forming process. This comparison aims to evaluate the accuracy and dependability of numerical predictions compared to actual measurements during experimental roll forming.

2 Methodology

2.1 Material characterization

2.1.1 Uniaxial tensile test

In this research, data for yield stress, elastic modulus, flow diagram, and Lankford coefficients were obtained by conducting uniaxial tensile tests following the ASTM-E8 standard. To ensure repeatability and minimize errors arising from the tensile tests, three samples were produced in each direction: rolling direction, transverse, and diagonal toward the rolling direction.

The digital image correlation (DIC) method was employed to derive the flow curve and strains in the width and thickness of the tensile test specimens to measure the plastic strain ratio. A random spot pattern was applied to the test specimen area, and the GOM correlate software was used to record longitudinal and transverse strain values during the test. Figure 2 visually represents the DIC test setup, including the sample size adhering to the standard guidelines. The digital image correlation method allowed for accurate strain measurements, determining essential material properties required to calibrate constitutive models in the roll-forming process.

The results of the uniaxial tensile tests conducted in three directions were analyzed and presented in the format of true stress and true strain, as shown in Fig. 3a. It is important to note that the stress–strain diagram obtained from the uniaxial tensile test is limited to lower strain values, typically in the range of 0.1 to 0.2. Beyond this range, necking of the specimen occurs, and the stress state is no longer uniaxial tension. On the other hand, the applied strains that cause deformation in the roll-forming process are mostly values

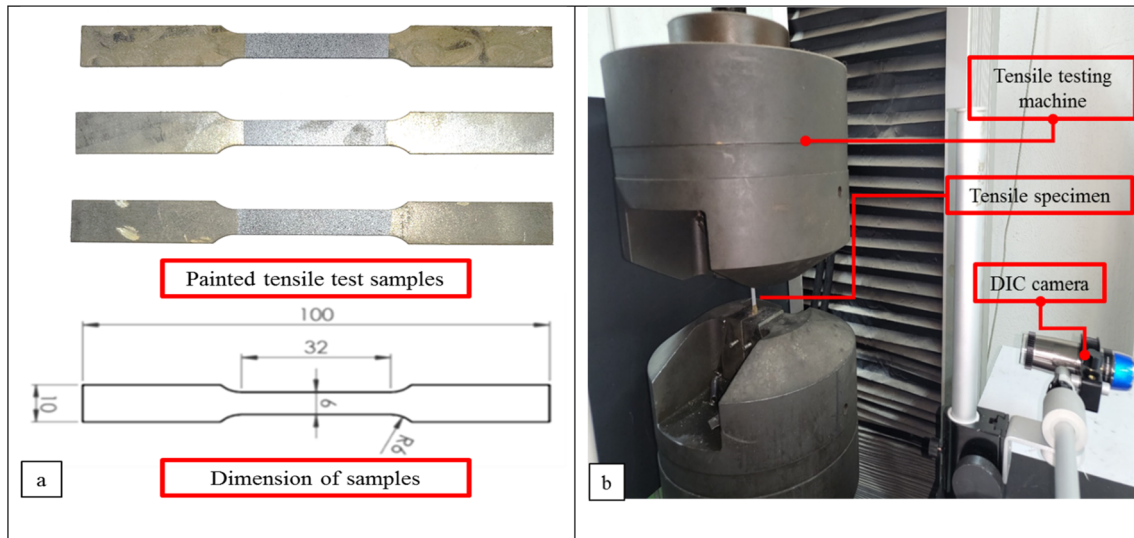


Fig. 2 **a** Tensile test samples (dimensions are in mm), **b** tensile testing equipment

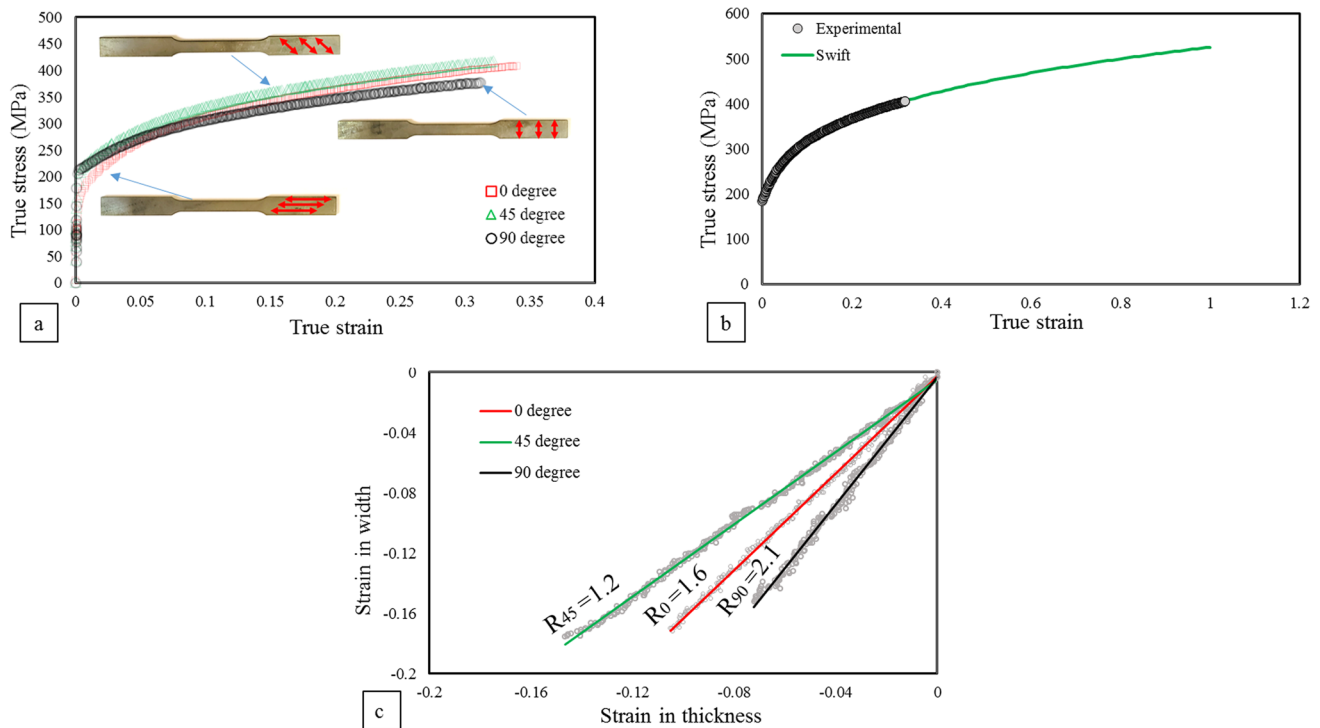


Fig. 3 **a** Stress–strain curve in rolling, transverse, and diagonal direction, **b** extrapolated flow curve based on swift hardening law, **c** width-to-thickness strain ratio and R -values

higher than the values that can be obtained from the uniaxial tensile test method (around 0.2), so it is necessary to estimate higher strain values with common models. According to the results of previous research, the Swift strain hardening model can provide accurate results to estimate the flow curve

at higher strain values, especially for describing the behavior of steel sheets [32–34]. So to extend the flow curve to higher strain values, the extrapolating method by the Swift strain hardening model is done [35]. The Swift curve, combined with the experimental true stress-true strain curve, is plotted

in Fig. 3b. This extrapolation allows for the representation of material behavior at higher strains, providing valuable insights into the material’s response beyond the limits of the uniaxial tensile test.

As per ASTM E517, the anisotropy variables in three directions were determined by plotting the ratio of transverse strain to thickness strain during the test. The graph created to calculate the anisotropy variables using line fitting with experimental data obtained through the DIC method is shown in Fig. 3c. In order to draw Fig. 3c, data points from the moment of plastic deformation occurs to a moment equal to 0.9 strain of necking point has been used. The slope of the fitted lines on the data points is reported with high accuracy because the coefficient of determination in all three directions is more than 99%.

Table 1 lists the mechanical properties of St12 steel, including elastic modulus, yield stress, Poisson’s ratio, and anisotropy coefficients. The normal anisotropy of St12, which represents the average of anisotropy coefficients for the sheet, is equal to 1.5. The values of the biaxial yield stress and the biaxial anisotropy coefficient were determined using the hydraulic bulge test and the Yld96 yield criterion, respectively (Table 1). These values provide crucial information for calibrating constitutive models in the numerical simulations for the roll-forming process.

2.1.2 Uniaxial loading–unloading-reloading (LUR) tensile test

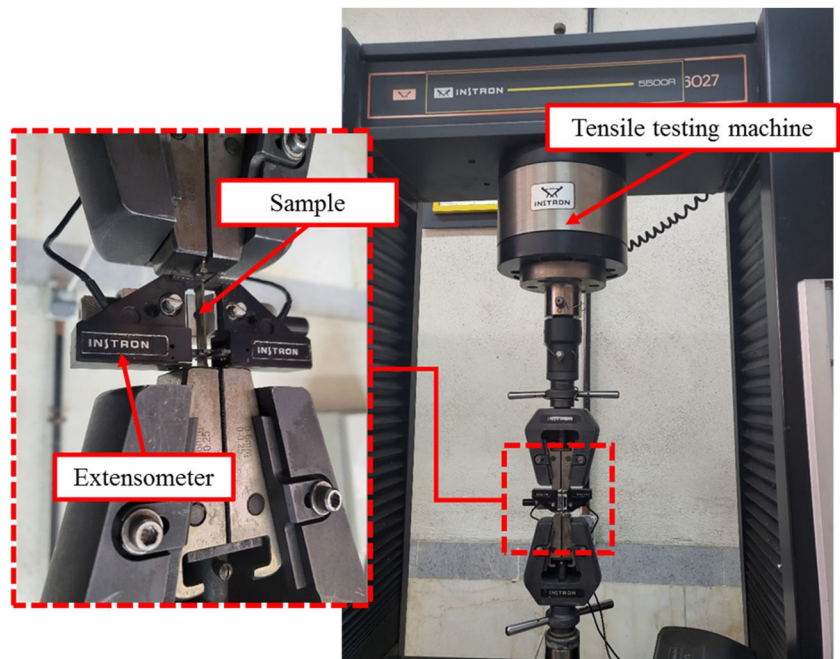
To assess the changes in elastic modulus resulting from plastic strain due to cyclic tensile loading, a loading–unloading–reloading test is performed on the St12 uniaxial tensile test sample. The test setup is depicted in Fig. 4, where extensometers measure strain with higher accuracy. The loading–unloading-reloading test examines the material’s response to repeated loading cycles and provides valuable information on its elastic behavior under various loading conditions. The data obtained from this test will be essential in understanding how the elastic modulus of St12 steel evolves throughout the plastic deformation process. It will contribute to more accurately representing its behavior in numerical simulations for roll-forming processes.

Figure 5 presents the true stress–strain diagram extracted from cyclic loading experiments to investigate the changes in elastic modulus with varying amounts of plastic strain. The chart was generated by subjecting the material to loading until reaching the presumed strain levels, then unloading it until the stress approached zero, followed by reloading to reach the next strain level. The predetermined pre-strain levels examined were 0.2%, 0.5%, 0.8%, 1%, 2%, 3%, 4%, 5%, 6%, 7%, 8%, 9%, and 10%. To capture the more significant

Table 1 Mechanical properties of St12

| E (GPa) | ν | σ_0 (MPa) | σ_{45} (MPa) | σ_{90} (MPa) | σ_b (MPa) | R_0 | R_{45} | R_{90} | R_b | R |
|-----------|-------|------------------|---------------------|---------------------|------------------|-------|----------|----------|-------|-----|
| 200 | 0.3 | 184 | 208 | 206 | 210 | 1.6 | 1.2 | 2.1 | 0.62 | 1.5 |

Fig. 4 LUR tensile test equipment



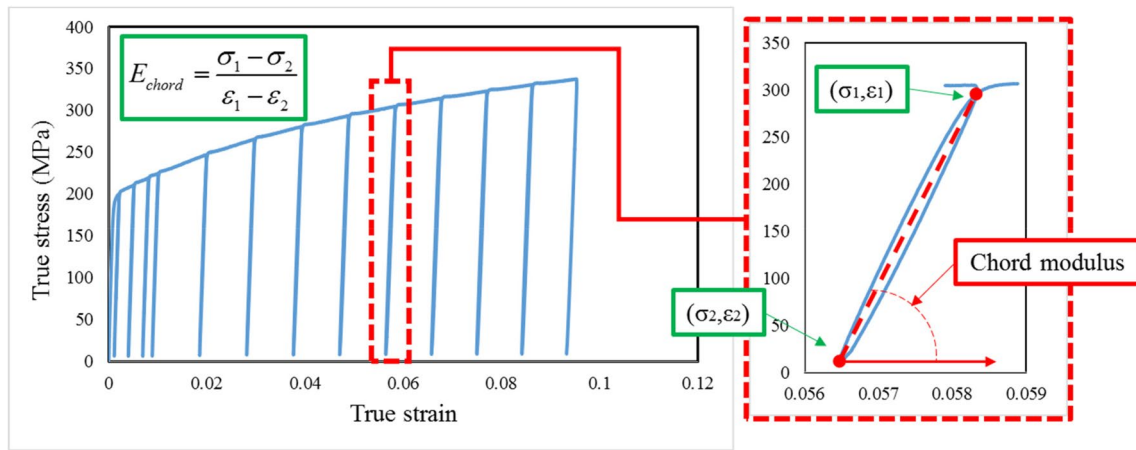


Fig. 5 Calculation of chord modulus based on LUR test results

changes in elastic modulus at lower pre-strains, the strains under 1% were investigated in three distinct levels.

This cyclic loading analysis provides valuable insights into how the elastic modulus of St12 steel evolves under various levels of plastic strain, contributing to a deeper understanding of its mechanical behavior during the roll-forming process. The data from Fig. 5 will aid in accurately calibrating the constitutive models used in numerical simulations, leading to more precise spring-back predictions and improved process control.

In the enlarged view of the diagram (Fig. 5), it becomes evident that the elastic modulus exhibits a nonlinear nature. Calculating the elastic modulus using the segment resulting from the loading curve slightly differs from the unloading elastic modulus. A common approach to derive the elastic modulus is to employ the “chord modulus” [27].

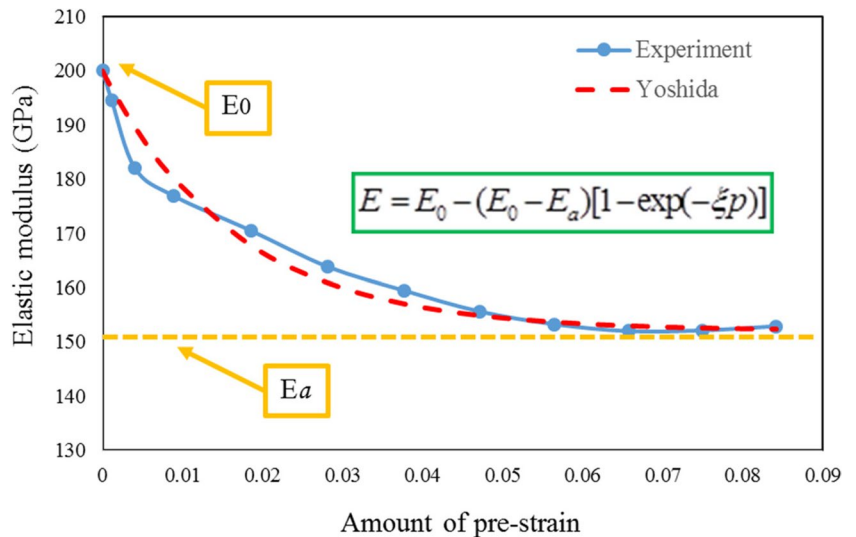
The calculated elastic modulus value will fall between the two loading and unloading moduli in this method.

The slope of the line resulting from the intersection of the loading and unloading curves will be determined as the elastic modulus. This chord modulus technique is widely used to estimate the elastic modulus within the plastic strain range explored during the cyclic loading experiments.

Based on the background of the research mentioned in the previous section, the decrease in elastic modulus exhibits a saturation phenomenon, wherein the reduction of elastic modulus reaches a point where it no longer changes with the increase of plastic strain and stabilizes at a saturation value. This behavior is evident in Fig. 6.

To model the reduction of elastic modulus with increasing plastic strain, Yoshida [18] proposed an equation that includes an exponential function to capture the saturation phenomenon. The equation to describe the variation of Young’s modulus is as follows:

Fig. 6 Elastic modulus variation vs. plastic strain



$$E = E_0 - (E_0 - E_a)[1 - \exp(-\xi p)] \tag{1}$$

By fitting Eq. 1 to the experimental data, the values of the variables in Yoshida’s equation were obtained, as presented in Table 2. In Yoshida’s equation (Eq. 1), the parameter represents the initial modulus, E_a represents the saturation value, and p represents the plastic strain. The initial modulus E_0 is the value of the elastic modulus of the initial sheet reported in Table 1.

The agreement of the experimental results with the values fitted by the Yoshida equation exhibited excellent agreement, with a coefficient of determination of approximately 97%. This agreement indicates that the proposed Yoshida equation provides an excellent fit for the experimental data, accurately capturing the saturation phenomenon in the elastic modulus variation with increasing plastic strain. The model’s ability to replicate the experimental results with high fidelity ensures its reliability and suitability for predicting the elastic modulus behavior in the roll-forming process for pre-punched profiles.

2.1.3 Hydraulic bulge test

Following the standard ISO 16808, the hydraulic bulge test was conducted to determine the biaxial yield stress value. The test was performed using a specialized machine depicted in Fig. 7, equipped with a hydraulic pump to supply sufficient oil pressure for sheet forming. The machine consists of a die, a blank holder, and a linear potentiometer to accurately measure the dome height during the test.

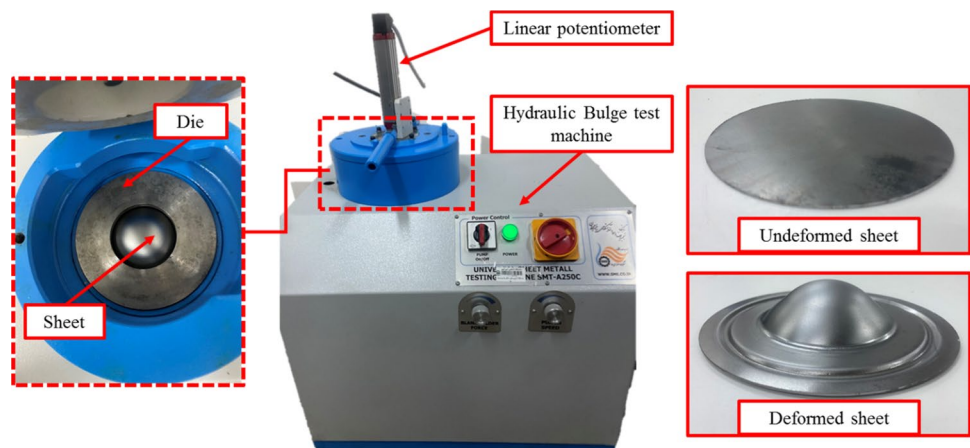
To calculate stress and strain bulge curvature radius (ρ) and instantaneous thickness of sheet (t) based on pressure of bulge (P) and height of bulge dome (h_d) that was measured by linear potentiometer calculated using Eq. 2 [36]:

$$\rho = \frac{r_c^2 + h_d^2}{2h_d}; t = t_0 \left[\frac{(r_c/\rho)}{\sin^{-1}(r_c/\rho)} \right]^2 \tag{2}$$

Table 2 Value of parameters for material models

| Material model | Material parameters | | | | | | | | |
|----------------|--------------------------|--------------------|------------------------|--------------------|--------------------|--------------------|--------------------|--------------------|--|
| Swift model | $K(\text{MPa})$ 524.4 | n 0.228 | ϵ_0 0.0083 | | | | | | |
| Yoshida model | E_a 152 | ξ 60.14 | | | | | | | |
| Hill48-R | F 0.2930 | G 0.3846 | H 0.6154 | N 1.1520 | | | | | |
| Hill48-S | F 0.1818 | G 0.3846 | H 0.6154 | N 1.2831 | | | | | |
| Yld89-R | a 0.7087 | c 1.2913 | h 0.9531 | p 0.8793 | | | | | |
| Yld89-S | a 0.7987 | c 1.2013 | h 1.12 | p 1.1447 | | | | | |
| Yld2000-2d | α_1 1.21 | α_2 0.76 | α_3 0.79 | α_4 0.85 | α_5 0.91 | α_6 0.92 | α_7 0.90 | α_8 0.86 | |

Fig. 7 Hydraulic bulge test machine (left) and formed parts (right)



In Eq. 2, r_c is the radius of the die, and t_0 is the initial thickness of the sheet. By using the instantaneous thickness and radius of curvature of the bulge, equivalent stress ($\bar{\sigma}$) and equivalent strain ($\bar{\epsilon}$) can be calculated from Eq. 3:

$$\bar{\sigma} = \frac{P\rho}{2t}; \bar{\epsilon} = \ln\left(\frac{t_0}{t}\right) \tag{3}$$

2.2 Material mathematical model

2.2.1 Hill 1948 yield criterion

The Huber-Mises-Hencky criterion was generalized by Hill [37] in 1948 to account for anisotropic materials. The anisotropic yield criterion involves the consideration of three orthogonal symmetry planes that collectively represent the anisotropy of the material. The yield criterion, as given in Eq. 4:

$$F(\sigma_{22} - \sigma_{33})^2 + G(\sigma_{33} - \sigma_{11})^2 + H(\sigma_{11} - \sigma_{22})^2 + 2L\sigma_{23}^2 + 2M\sigma_{31}^2 + 2N\sigma_{12}^2 = 1 \tag{4}$$

In this paper, the anisotropic axes are denoted as 1, 2, and 3, with the constants $F, G, H, L, M,$ and N being specific to the material’s anisotropic state. Axis 1 is often aligned with the rolling direction, axis 2 is aligned with the transverse direction, and axis 3 is collinear with the normal direction of the sheet metal.

The paper adopts two distinct approaches to determine the anisotropy parameters for Hill’s 1948 model. The first approach, Hill’48-R, uses the r values obtained from three uniaxial tension tests. These r values are essential for characterizing the anisotropic behavior of the material.

The second method, known as Hill’48-S, relies on employing the yield stresses obtained from three uniaxial tension tests. These yield stresses play a key role in defining the anisotropic yield criterion for the material.

2.2.2 Yld89 yield criterion

Barlat and Lian [38] proposed a more general form of Hosford’s criterion by extending it to materials exhibiting planar anisotropy in the form:

$$f = a|k_1 + k_2|^M + a|k_1 - k_2|^M + c|2k_2|^M = 2\sigma_e^M \tag{5}$$

where k_1 and k_2 are defined as:

$$k_1 = \frac{\sigma_{11} + h\sigma_{22}}{2}; k_2 = \left[\left(\frac{\sigma_{11} - h\sigma_{22}}{2} \right)^2 + p^2\sigma_{12}^2 \right]^{1/2} \tag{6}$$

This paper determined yield function coefficients $a, c, h,$ and p using two approaches similar to Hill’s 1948 methodology. Anisotropy R -values in three directions ($0^\circ, 45^\circ,$ and 90°) are used

for the first approach. The second method uses the three yield stresses ($\sigma_0, \sigma_{45},$ and σ_{90}) to determine yield function coefficients.

2.2.3 Yld2000-2d yield criterion

The Yld2000-2d function is designed to provide a more accurate and robust approach for modeling the yield behavior of anisotropic materials. By simplifying the analytical complexity and improving the numerical methods for obtaining anisotropy coefficients, the Yld2000-2d function seeks to overcome the limitations of Yld96 and offer a more practical and accurate alternative for yield prediction in metal sheets.

The Yld2000-2d yield function can be calculated based on the following relations:

$$\phi = \phi' + \phi'' = 2\bar{\sigma}^a \tag{7}$$

In Eq. 7, the variable “ a ” is a coefficient based on the material’s structure, according to Hosford’s paper, equals 6 for materials with a BCC structure, such as steel, and 8 for materials with an FCC structure, such as aluminum [39].

$$\phi' = |X'_1 - X'_2|^a, \phi'' = |2X''_2 + X''_1|^a + |2X''_1 + X''_2|^a \tag{8}$$

The isotropic functions presented in Eq. 8 can be calculated based on the following equation using X_{ij} values, which are linear transformations of stress values.

$$X_1 = \frac{1}{2}(X_{xx} + X_{yy} + \sqrt{(X_{xx} - X_{yy})^2 + 4X_{xy}^2})$$

$$X_2 = \frac{1}{2}(X_{xx} + X_{yy} - \sqrt{(X_{xx} - X_{yy})^2 + 4X_{xy}^2}) \tag{9}$$

The Cauchy stress values can be converted to X values using the linear transformation matrix L' and L'' .

$$\begin{cases} X' = L' \cdot \sigma \\ X'' = L'' \cdot \sigma \end{cases} \tag{10}$$

The values of linear conversion functions can be calculated using α input values, which can be extracted from the material properties by standard mechanical tests.

$$\begin{bmatrix} L'_{11} \\ L'_{12} \\ L'_{21} \\ L'_{22} \\ L'_{66} \end{bmatrix} = \begin{bmatrix} \frac{2}{3} & 0 & 0 \\ -\frac{1}{3} & 0 & 0 \\ 0 & -\frac{1}{3} & 0 \\ 0 & \frac{2}{3} & 0 \\ 0 & 0 & 1 \end{bmatrix} \begin{bmatrix} \alpha_1 \\ \alpha_2 \\ \alpha_7 \end{bmatrix}$$

$$\begin{bmatrix} L''_{11} \\ L''_{12} \\ L''_{21} \\ L''_{22} \\ L''_{66} \end{bmatrix} = \frac{1}{9} \begin{bmatrix} -2 & 2 & 8 & -2 & 0 \\ 1 & -4 & -4 & 4 & 0 \\ 4 & -4 & -4 & 1 & 0 \\ -2 & 8 & 2 & -2 & 0 \\ 0 & 0 & 0 & 0 & 9 \end{bmatrix} \begin{bmatrix} \alpha_3 \\ \alpha_4 \\ \alpha_5 \\ \alpha_6 \\ \alpha_8 \end{bmatrix} \tag{11}$$

The variables of α_1 to α_6 will be obtained using six variables obtained from uniaxial tensile tests in the rolling direction, transverse and diagonal directions toward the rolling direction, resulting in three anisotropic variables R_0, R_{45}, R_{90} , as well as three yield stresses in the three directions are σ_0, σ_{45} , and σ_{90} . The values of α_7 and α_8 were obtained based on biaxial yield stress σ_b and biaxial anisotropy R_b . The biaxial yield stress was obtained by hydraulic bulge test, and to determine biaxial anisotropy, another yield function Yld96 [37] was used as Barlat et al. [38] suggested.

2.2.4 Strain hardening

Swift’s strain-hardening law (Eq. 12) was utilized to fit the experimental stress–strain curve, allowing for estimating the flow curve after necking. This process was performed following the material properties of the sheet being tested.

$$\sigma = K(\epsilon_p + \epsilon_0)^n \tag{12}$$

In Eq. 12, the hardening strain power is equal to n . The initial strain is indicated by ϵ_0 , the plastic strain by ϵ_p , and the hardening strain coefficient by K . The Swift law was used to fit the experimentally measured stress–strain data presented in Table 2. The Swift unknown parameters values were obtained by applying the Swift equation to the data.

2.2.5 Parameters identification

An optimization method can be employed to minimize the discrepancies between the experimental data and the values predicted by the anisotropic yield functions to determine the values of the anisotropy coefficients. Optimization techniques for this purpose are well established and widely documented in the literature [40].

The interior algorithm [41, 42], a Matlab® optimization subroutine, was used in this research. The “Error” function is:

$$Error = W_\sigma \sum_{i=1}^m \left(\frac{\sigma_{model}}{\sigma_{exp}} - 1 \right)^2 + W_r \sum_{i=1}^m \left(\frac{r_{model}}{r_{exp}} - 1 \right)^2 \tag{13}$$

where the superscripts “*exp*” and “*model*” in Eq. (13) signify quantities that have been measured or that are expected based on an anisotropic yield function. Additionally, “ m ” represents the number of available experimental data points, while “ w_σ ” and “ w_r ” stand for the weighting values for stresses and R -values, respectively. In this study, the

maximum number of iterations is set to 100,000, the weighting factors are set to 1, and the tolerance for error function is set to $1e - 24$.

3 Experimental method

A 1-mm-thick St12 sheet was used in the roll-forming procedure. The study investigated the influence of holes on the amount of spring-back during the roll-forming process by conducting experiments with a flower pattern consisting of three forming stations and a channel-shaped section. The profile was formed into a 45° channel, with angles of 15° in the first station, 30° in the second station, and 45° in the final station. The flower pattern of the channel section is illustrated in Fig. 8.

The flower pattern was created using the fixed bending radius method with a bending radius of 2 mm. To ensure proper sheet engagement between the two stations at any point and correct guidance to the next station, the length of the profile should be larger than twice the distance between the two stations, approximately 40 cm. Setting the sample length at 120 cm addressed two main issues during the roll-forming process. Firstly, it was chosen to ensure proper sheet guidance between the forming stations. With a longer length, the sheet remains well guided throughout the forming process, reducing the risk of misalignment or other problems with shorter samples.

Secondly, the longer sample length was selected to avoid measuring spring-back at the very beginning and end of the sheet. A common defect known as “end flare” can occur at these locations. End flare refers to the deformation of the material near the edges of the sheet, which can lead to inaccuracies in measuring spring-back and affect the overall accuracy of the experimental data.

The study used three samples to investigate the effects of holes and their placement. The first sample had no holes, the second sample had holes in the center of the profile’s bend area, and the third sample had holes on the profile’s flange just outside the bend area. These three samples were the focus of the investigation, as shown in Fig. 9.

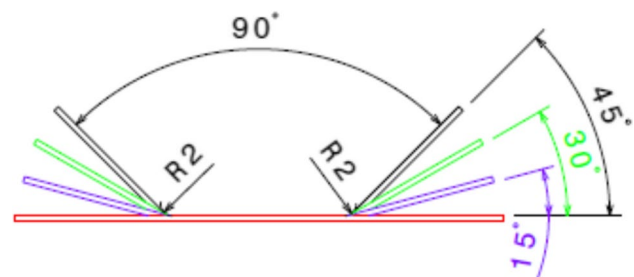


Fig. 8 Flower pattern of roll forming

Throughout the rest of the essay, the first sample with no holes will be called “without holes.” The second sample, with holes in the center of the profile’s bend area, will be called “on the bend.” Lastly, the third sample, with holes near the profile’s bend area on the flange, will be referred to as “near the bend.”

Sheet metal samples’ geometrical variables and roll-forming process parameters used in the experimental procedure are listed in Table 3.

Figure 10 illustrates the roll forming line and the rollers used. The roll forming line consisted of three forming stations, each including two rollers. A guiding system with four rollers, two on each side, was employed to guide the sheet into the first forming station. There was no gap between the top and bottom rollers, and the distance between the upper and lower rollers was equal to the thickness of the sheet metal. Notably, the upper roller covered only the channel’s web, while the lower roll completely enclosed it, as depicted in Fig. 10b.

Figure 11 showcases the profiles produced with and without holes during the cold roll-forming process at three forming stations. The process was stopped when a portion of the profile had passed the 45° station but remained under the first forming station. At this point, the profile was taken out from the machine for further analysis. The resulting profile has three different sections: a bend of 15° at the start, 30° in the middle, and 45° at the finish. As a result, the angles of the three forming stations on the profile can be measured, allowing for the determination of spring-back angles at all three roll-forming stations.

A Johansson coordinate measuring machine was employed to measure the coordinates and accurately gauge

Table 3 Sheet metal samples geometrical values and roll-forming process parameter

| Parameter | Unit | Value |
|---------------------------|--------|-------|
| Sheet length | mm | 1200 |
| Sheet width | mm | 85 |
| Sheet thickness | mm | 1 |
| Bend angle | Degree | 45 |
| Bend radius | mm | 2 |
| Hole diameter | mm | 15 |
| Distance between holes | mm | 35 |
| Roll diameter | mm | 93 |
| Distance between stations | mm | 395 |
| Top roll width | mm | 30 |
| Friction coefficient | - | 0.2 |

the amount of spring-back. Three cross-sections were used for each target site to ensure precise measurements, and the results represent the average data of these three cross-sections. The cold roll-formed profiles were then measured using the Johansson coordinate measuring machine. The spring-back of the profiles was calculated by subtracting the measured angle from the ideal angle, as defined by Eq. 14.

$$\Delta\theta = \theta_i - \theta_m \quad (14)$$

The variable θ_i in Eq. 14, which represents the ideal angle, is equal to 15, 30, and 45° at the first, second, and third stations. The variable θ_m also denotes the angle determined by the coordinate measurement equipment.

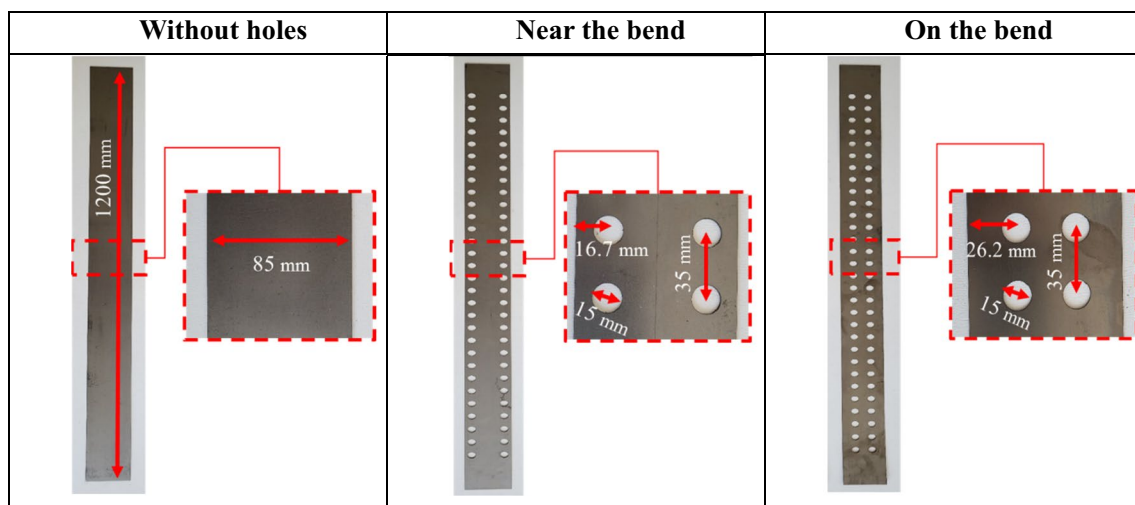


Fig. 9 Cold roll-forming samples

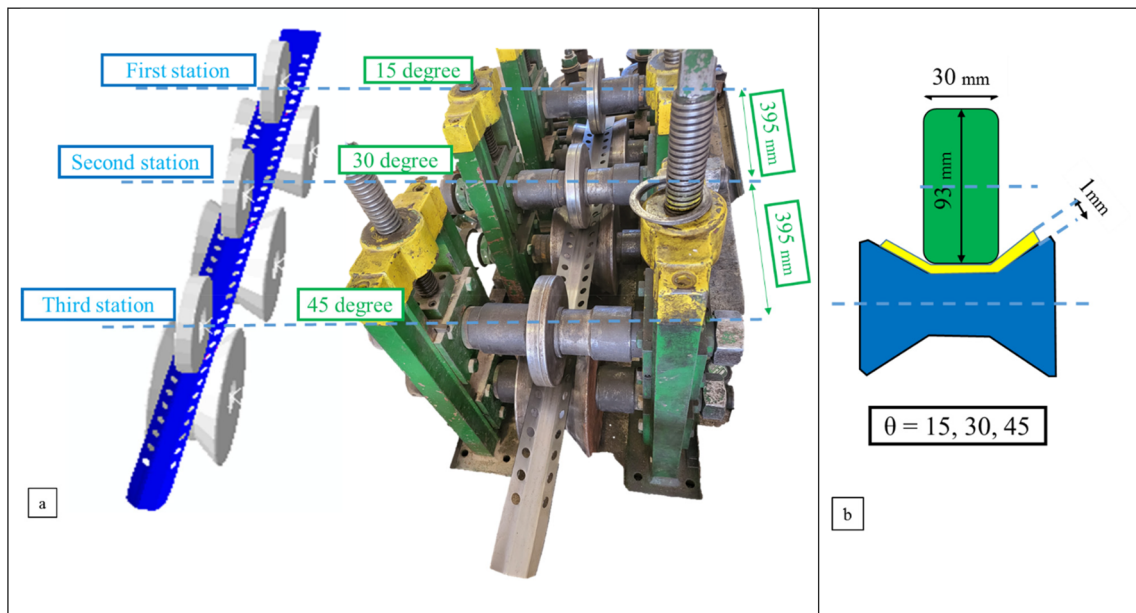


Fig. 10 a Roll forming equipment, b roll forming setup dimensions

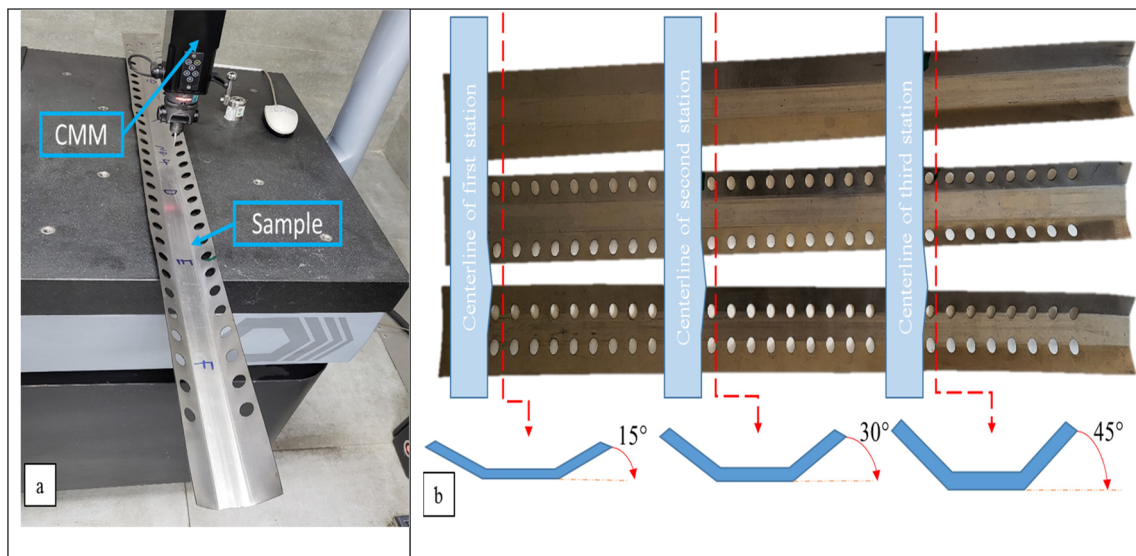


Fig. 11 a Coordinate measuring machine used to measure the angle of profile after spring-back, b roll-formed profiles

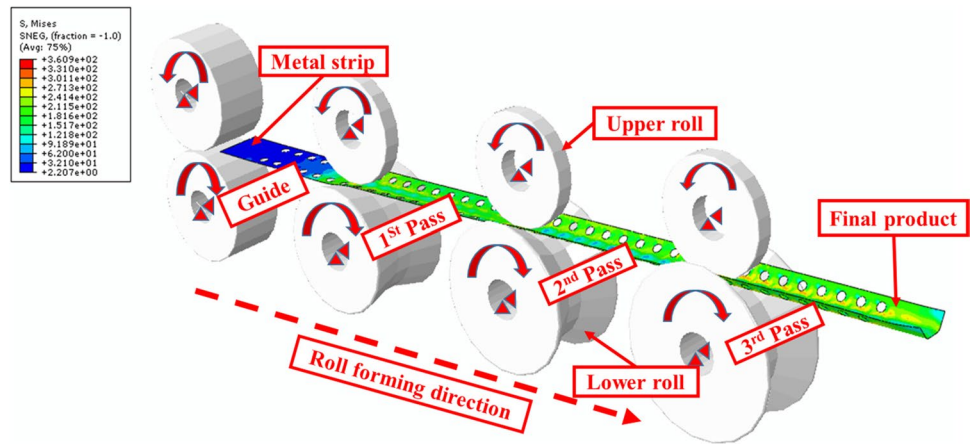
4 Numerical method

The spring-back was determined by numerical simulations of the roll-forming process using the Abaqus finite element software. Figure 12 illustrates a perspective of

the roll-forming procedure, which comprises three forming stations and one guiding station, as represented in the finite element software.

Based on the results of past research, it is true that using solid elements can show the through-thickness effects, including changes in sheet thickness, but it will significantly

Fig. 12 FEA model of the roll-forming process



increase the computation time [43]. Also, considering that roll forming is a plane stress process, previous research has shown that using a shell element with a sufficient number of integral points through thickness has an acceptable accuracy in spring-back prediction, taking into account less computational time [34]. Earlier studies have shown that good simulation results can be obtained using the S4R four-node shell element with between 5 and 9 integration points [44, 45]. The sheet was modeled using the S4R shell element with four reduced integral nodes.

An explicit dynamic solver was employed due to its suitability for complex deformations and contact surfaces inherent in the roll-forming process [46]. By ensuring that the internal energy to kinetic energy ratio remained below 5% throughout the simulation, we validated that the process was modeled under quasi-static conditions despite using an explicit scheme. This approach ensured that the results reflected the steady-state behavior of the material without significant dynamic effects. In mesh sensitivity analysis, when the number of elements equals 5100 elements, the slope of the changes in the maximum strain and equivalent stress is less than 2%. According to that, the number of suitable elements for finite element simulation, considering the solving time and accuracy, was 5100 elements.

A finer mesh was used in the bend region to accurately represent the bending operation in the bending zone and the intensification of plastic strain. Additionally, since the deformation gradient in the profile's transverse direction is several times greater than that in the longitudinal direction, a finer mesh gradient was employed in the transverse direction. The mesh surrounding the holes was also refined to account for stress concentration in that area.

In the roll forming simulation, the profile's angle was calculated using the coordinates of a collection of nodes “*k*” on the profile's flange, as specified by Eq. 15 [34].

$$Slope(radian) = \sum_{n=1}^k (y_n - \bar{y}) / (x_n - \bar{x}); \theta_m(\text{deg.}) = \arctan(slope) \cdot 180/\pi \quad (15)$$

where \bar{x} and \bar{y} are the mean average values of x and y , respectively. θ_m is the measured angle value obtained by a numerical method subtracted from the ideal angle to calculate spring-back as in Eq. 14.

The material properties were defined in the finite element simulation using different yield criteria, including Von Mises isotropic yield criterion, Hill1948, Yld89, and Yld2000-2d anisotropic yield criteria. The Swift model described the flow curve, and isotropic hardening was considered. For Yld89 and Hill1948, two calibration methods were used based on yield stress and R -values. In the case of Yld89_R and Yld2000-2d, the elastic modulus was considered variable, while it was assumed to be constant for other cases. The plastic behavior of material models (Yld89, Yld2000-2d, Yoshida) that were not included in the standard Abaqus software were incorporated into finite element analysis using the “VUMAT” user-defined material function.

The forming rollers were defined as rigid bodies with one degree of freedom to rotate around their axis, and the degrees of freedom of the sheet were not constrained. The distance between the two rollers is equal to the thickness of the sheet, and there is friction contact between the sheet and the rollers, which causes the sheet to move and shape with the rotation of the rollers. The Coulomb model with a friction coefficient of 0.2 was used to compute the friction between the sheet and the rolls [47].

There are different parameters that may have effects on the model in every study on processes like roll forming including temperature, elastic flattening of rollers, and friction coefficient. Each of these parameters can be changed and have a small effect on the behavior of the model. For example, considering the flattening of the rollers can make changes, however small, in the contact conditions and

material flow in forming. Also, the change in temperature can have effects on the material’s behavior under deformation, however small. In this article, the effect of changes in the coefficient of friction and temperature, as well as the flattening of the rollers, has been ignored. It is worth mentioning that due to the possibility of influencing these parameters on the amount of spring-back and the accuracy of its prediction, inspection of the effects of those parameters is beyond the scope of this article, and it is suggested to be investigated in future research.

5 Results and discussion

In the current study, a comprehensive investigation was conducted to examine how the modeling procedure for material plastic behavior affects the accuracy of predicting spring-back in the roll-forming process. It is worth noting that, according to Talebi et al. [14], the deformation mechanism in the cold roll-forming process for profiles without holes is characterized by plane strain deformation. However, a heterogeneous deformation mechanism is anticipated when it comes to pre-punched profiles. This divergence can be attributed to the impact of the hole on the stresses and

strains in the vicinity of the hole, subsequently affecting the overall deformation state within this specific region. Given the deformation mechanism, it can be concluded that for pre-punched profiles, a yield criterion with accurate results based on experimental values in different deformation mechanisms (biaxial and uniaxial tensile deformation and pure shear) should be used to predict spring-back accurately. In comparison, employing reasonable, less complex yield criteria that offer acceptable results for plane strain deformation in the cold roll-forming process for simple holeless profiles is conceivable.

Figure 13 presents the measured spring-back based on simulation results obtained using four different yield criteria calibrated using the two mentioned approaches. It is worth noting that bowing and twisting are not within the scope of this article. Since the angle measurement for spring-back calculation is conducted on the cross-section of U-shaped profiles, the analysis does not explicitly consider bowing and twisting effects. Therefore, the results presented in Fig. 13 focus solely on spring-back deformation without accounting for bowing or twisting caused by spring-back. In the simulations, the elastic modulus variation was considered for Yld89_R and Yld2000-2d yield criteria, as indicated by the orange bars labeled Yld89_R + E and Yld2000-2d + E.

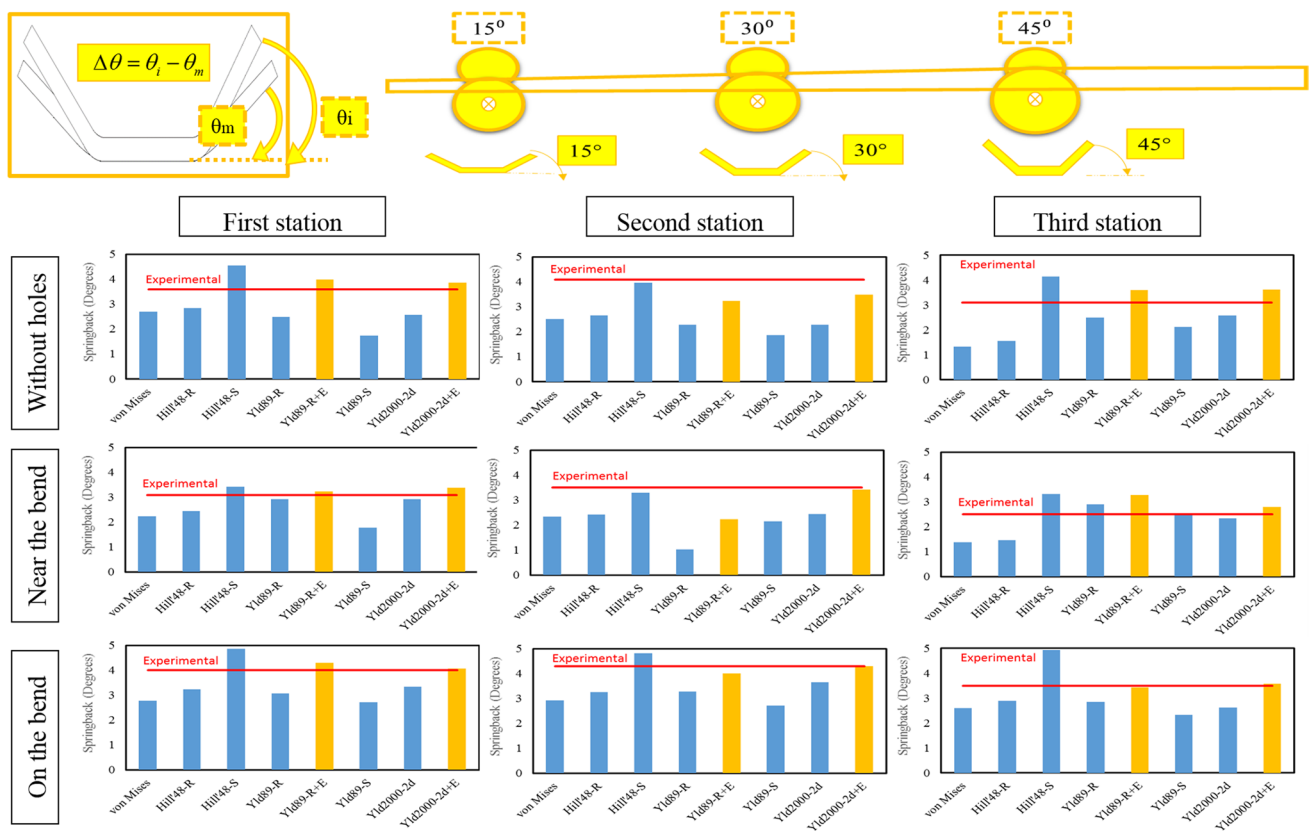


Fig. 13 The amount of spring-back based on simulation results by different constitutive models for three samples in each forming station

The reason for considering the elastic modulus variation on the two mentioned yield criteria is to calculate the influence of plastic pre-strain on the elastic modulus. As shown in Sect. 2.1.2, the elastic modulus decreases with the increase in plastic strain, and there is an exponential decreasing trend until the saturation region. Since the cold roll-forming process is a stepwise deformation process, the amount of plastic strain applied to the steel profile in the previous forming station reduces elastic modulus in the deformation area and thus affects the amount of spring-back. Since the yield criteria, Yld2000-2d and Yld89_R, have more input parameters and flexibility and are expected to provide more accurate results, the elastic modulus changes were considered on these two. The red line represents the experimental value of spring-back, making it easy to identify the differences between the experimental and numerical spring-back values. The comparison between the two calibrated Hill48 yield criteria (Hill48_R and Hill48_S) and the two calibrated Yld89 yield criteria (Yld89_R and Yld89_S) reveals distinct patterns in the predicted spring-back results. Specifically, the spring-back values predicted by Hill48_S are consistently higher than those predicted by Hill48_R for all three samples and forming stations.

This observation suggests that the choice of calibration method significantly affects the accuracy of the Hill48 yield criterion in predicting spring-back. On the other hand, in the case of the Yld89 yield criterion, the calibration method also plays a crucial role in predicting spring-back. The yield criterion calibrated by anisotropy R -values (Yld89_R) consistently predicts higher spring-back values than the yield criterion calibrated by yield stresses (Yld89_S) in all three cases and all forming stations.

The observed discrepancy between the spring-back predicted by Hill48_S and the experimental value and the underestimation of spring-back for other yield criteria with constant elastic modulus can be attributed to the neglect of elastic modulus variation in the simulations. As mentioned, the elastic modulus decreases with plastic strain accumulation during the roll-forming process. This reduction in elastic modulus leads to a higher amount of elastic strain being released, resulting in increased spring-back.

Figure 14a illustrates that Hill48 and Yld89 criteria, calibrated using R -values, can accurately predict the anisotropy values in rolling, transverse, and diagonal directions (0, 45, and 90°), which aligns with the expected behavior. However, these criteria show some deviation from the experimental values when predicting yield stresses at 45 and 90° to the rolling direction. On the other hand, Fig. 14b demonstrates that criteria calibrated with yield stresses can precisely predict the yield stresses, matching the experimental values as expected. However, when predicting the R -values, they deviate from the experimental values.

In contrast, the Yld2000-2d criterion, which is a more flexible yield criterion that can be calibrated using both anisotropy values and yield stresses as experimental input parameters, accurately predicts both the R -values and yield stresses at all three angles (0, 45, and 90°), following the experimental values.

Figure 14c shows the yield surfaces for the four yield functions used in the finite element simulation. Additionally, the experimental values for the yield stress obtained from tensile tests in the rolling direction, transverse direction, and the biaxial yield stress measured by the bulge test are indicated on the chart. The yield surface represents the range of the elastic region, and a larger yield surface can lead to higher elastic strain and, consequently, higher spring-back. The graph shows that the Hill48_S yield function has the largest yield surface among the four functions. Based on the spring-back results, it was observed that Hill48_S indeed produced the highest spring-back value, and the amount of spring-back was overestimated compared to the experimental values.

Indeed, the Yld2000-2d criterion is the best yield criterion among the four in accurately predicting yield stresses. It is unique because it can predict the biaxial yield stress value exactly, making it the most accurate. Yld2000-2d is calibrated with the biaxial yield stress experimental value, which explains why it performs so well in predicting this value. The yield surface chart further reinforces the superiority of Yld2000-2d in accurately predicting yield stresses. It exhibits the closest match to the experimental yield stress values compared to the other yield functions, with Yld89_R coming second in proximity to experimental values after Yld2000-2d.

Figure 15 presents the variation of Young's modulus in three different models: "on the bend," "without holes," and "near the bend" along the length of the profiles. The elastic modulus variation is plotted for three distinct zones of the profile: (1) the middle of the flange, (2) the middle of the bending zone, and (3) the middle of the web. For the flange and web of the profile, the results of elastic modulus variation are obtained from the top surface of the profile. However, the results are collected from the profile's middle and top surfaces for the bending zone because the bending zone is critical in influencing the spring-back behavior.

The analysis of Fig. 15 indicates that the most significant decrease in Young's modulus is observed in the "without holes" profile across all three investigated areas (middle of the flange, bending zone, and middle of the web). On the other hand, the "on the bend" profile exhibits the most negligible change in Young's modulus in the web and flange areas.

In the bending zone, a critical area influencing spring-back, the "near the bend" profile shows the lowest changes

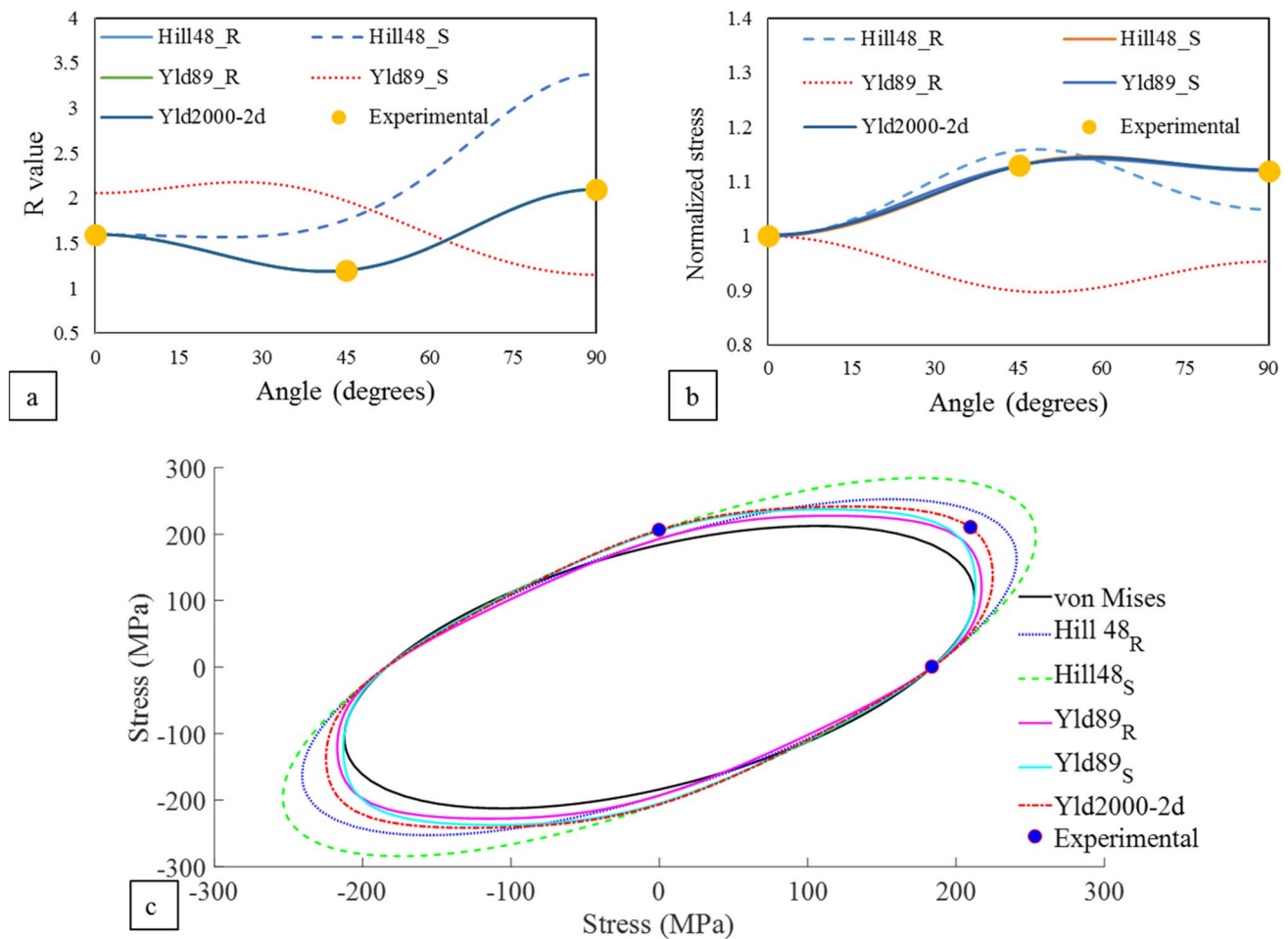


Fig. 14 **a** *R*-value predicted by different yield criteria in different angles from rolling direction. **b** Normalized yield stress predicted in different angles toward rolling direction. **c** Yield surfaces of different yield criteria

in Young’s modulus in both the top surface and the middle layer of the sheet thickness. Considering the spring-back results presented in Fig. 13, it can be observed that the variation of elastic modulus has the most negligible impact on the “near the bend” profile, as indicated by the minor difference between the spring-back values for the Yld2000-2d and Yld2000-2d + E constitutive models in comparison to the “on the bend” and “without holes” profiles. This finding can be attributed to the information provided in graph number 2 of Fig. 15, which shows that the elastic modulus variation in the “near the bend” profile is relatively lower than in the other profiles.

A predicting error determination technique is used in this research to address better the effect of constitutive modeling on spring-back prediction accuracy. The most accurate constitutive model for each sample can be recognized using this technique, with eight constitutive models investigated in this paper.

In statistics, the mean absolute percentage error (MAPE) [48], often referred to as the mean absolute

percentage deviation (MAPD), is a metric for predicting technique accuracy. The accuracy is often expressed as a ratio determined by Eq. 16 [49]:

$$MAPE = \frac{100\%}{n} \sum_{i=1}^n \left| \frac{A_i - F_i}{A_i} \right| \tag{16}$$

where A_i denotes the real value and F_i denotes the predicted value. This ratio’s absolute value is added for each predicted data point and then divided by the number of data points.

Figure 16 provides a comprehensive assessment of the precision of spring-back prediction by calculating the mean absolute percentage error (MAPE) for the four yield surfaces. The evaluation considers factors such as the anisotropy of the yield criterion, the calibration method, and the impact of varying elastic modulus in different hole position scenarios.

In a general overview, when not considering variation in elastic modulus, the most accurate anisotropic yield criteria for predicting spring-back in all three profiles are

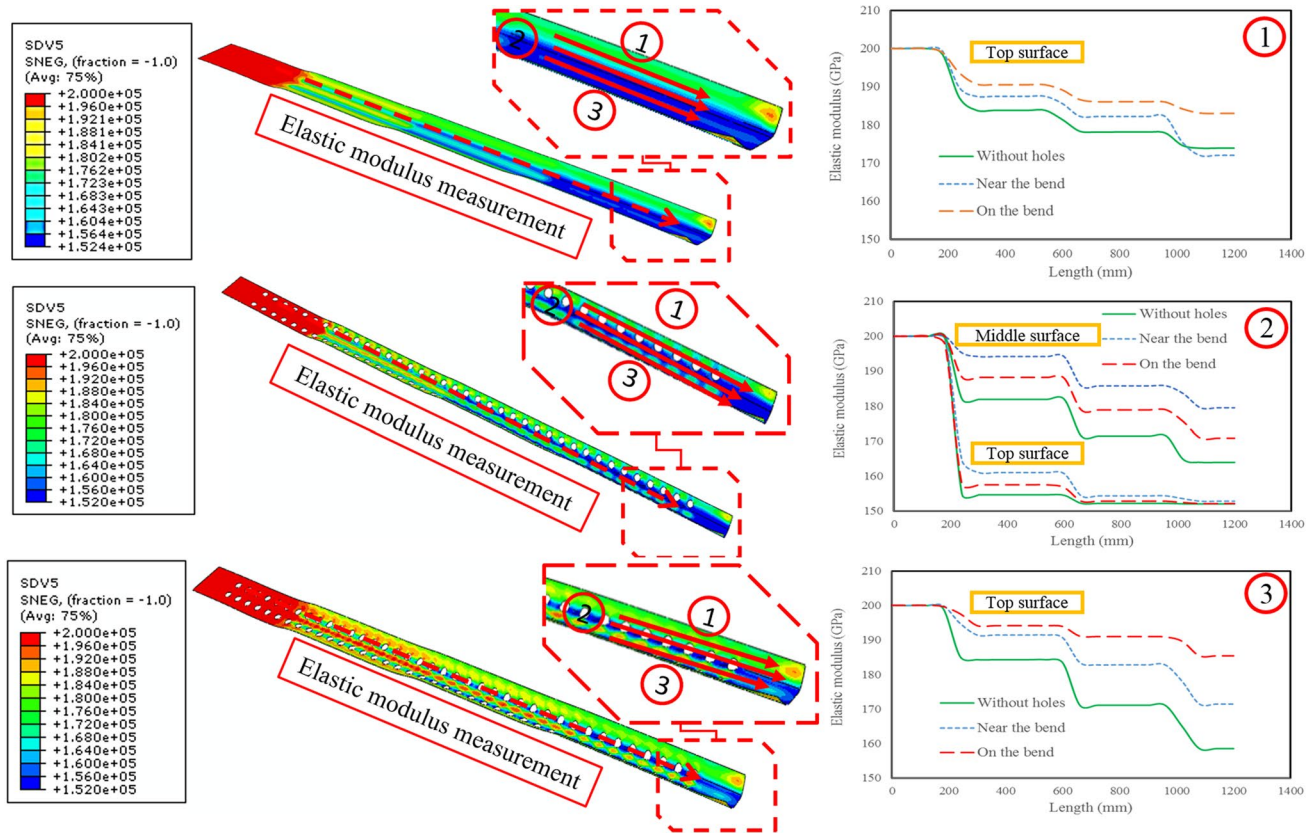


Fig. 15 Variation of elastic modulus in various samples: (1) the bend zone, (2) middle of flange zone, (3) the middle of web of profiles

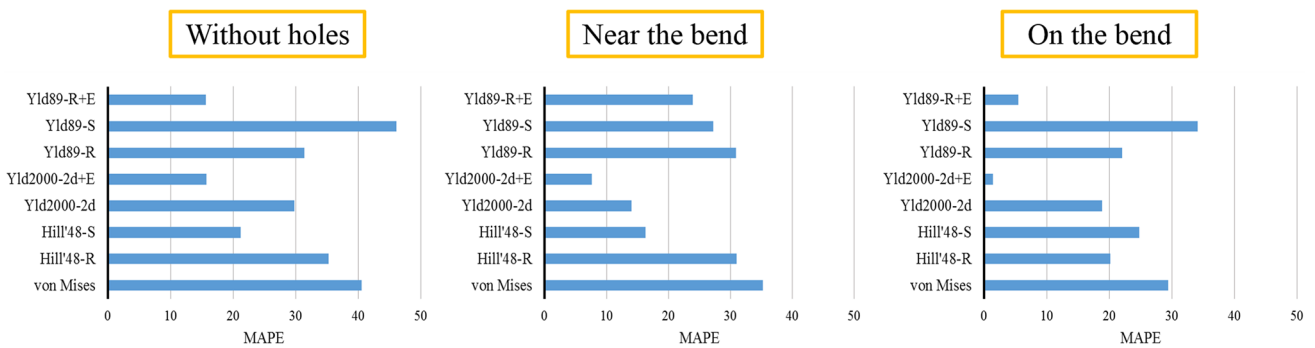


Fig. 16 Mean absolute spring-back prediction error of the proposed model regarding various yield criteria

Yld2000-2d and Hill48-S, with a relatively low MAPE of about 20%. However, it is worth noting that Hill48-S tends to over-predict the amount of spring-back compared to the experimental value, which can be attributed to its larger yield surface, as demonstrated in Fig. 14. On the other hand, Yld2000-2d yields under-predicted spring-back values, mainly due to its neglect of the effect of decreasing elastic modulus. This indicates the significance of considering the elastic modulus variation in accurately predicting spring-back.

Based on the consideration of elastic modulus variation in the constitutive model, the Yld2000-2d + E model appears to be the best yield criterion for all three profiles, with an average MAPE of about 8% (as shown in Fig. 16). This model outperforms other yield criteria in terms of accuracy in predicting spring-back. Following closely, the Yld89_R + E model, which incorporates the effect of elastic modulus change and is the nearest to the Yld2000-2d model (as demonstrated in Fig. 14), is the second best with an average MAPE of about 15% for all three profiles. On the other

hand, the isotropic Von Mises and anisotropic Yld89_S yield criteria showed the highest MAPE values. The Von Mises disability and Yld89_S inaccuracy in the prediction of R -values contribute to their relatively high MAPE of about 35%.

By comparing the radar charts in Fig. 16, a decreasing trend of MAPE results can be observed from the “without holes” to the “near the bend” sample and from “near the bend” to “on the bend” sample for some criteria (Von Mises, Hill48_R, and Yld89_R). This trend suggests that the accuracy of the spring-back prediction tends to improve as the punched hole gets closer to the bend area. Furthermore, it can be concluded that the yield stress-based calibrated criteria, including Yld89_S and Hill48_S, provide more accurate results in the “near the bend” profile compared to the two other profiles. These criteria seem better suited for predicting spring-back in the bending zone. On the other hand, in the case of R -value calibrated criteria, which are Hill48_R and Yld89_R, the results show a lower MAPE for the “on the bend” profile than the two other profiles. This indicates that these criteria may better predict spring-back in the bend’s immediate vicinity.

In summary, the performance of different yield criteria in predicting spring-back can vary depending on the location of the profile concerning the bend area. Yield stress-based calibrated criteria appear more accurate in the “near the bend” profile, while R -value calibrated criteria show better accuracy in the “on the bend” profile. Overall, considering the variation of elastic modulus in the models (Yld89_R + E and Yld2000-2d + E) improves the accuracy of spring-back prediction for all three profiles. The results of the present study lay a necessary foundation for further research on the effects of specific model parameters, allowing for a more detailed understanding of how variations in these parameters influence the accuracy and reliability of predictions.

6 Conclusion

This study investigated the effect of the constitutive model on the accuracy of spring-back prediction for pre-punched profiles produced by the cold roll-forming process. The finite element analysis was performed using Abaqus with eight constitutive models. Constitutive models differ regarding yield criteria, yield function calibration, and elastic modulus variation consideration. Three samples made of St12 with 1 mm thickness, including a simple profile (without holes), a profile with holes in the bending zone (on the bend), and a profile with holes next to the bending zone (near the bend), were used to investigate the effect of holes and its position on spring-back. It is found:

- (1) Contrary to the Yld89 criterion, yield stress calibrated Hill48 predicts more spring-back than the R -values calibrated in all forming stations for three samples.
- (2) Unlike other yield criteria, Hill48_S predicts greater spring-back than the actual amount in all samples due to its bigger yield surface, indicating a wider range of elastic deformation.
- (3) The study reveals that the elastic modulus variation has the most negligible impact on the predicted spring-back for “near the bend” profile, with the lowest changes in elastic modulus in the bending zone at both the top and middle layer of sheet thickness.
- (4) The best anisotropic yield criteria to predict spring-back in all three profiles are Yld2000-2d and Hill48-S, which have a low MAPE of roughly 20%. It is worth noting that Hill48_S and Yld2000-2d respectively overestimate and underestimate the spring-back toward actual experimental value.
- (5) Considering elastic modulus variation in the constitutive model, the optimal yield criterion for all three profiles would be the Yld2000-2d + E model with a MAPE of roughly 8% as an average of three MAPE exhibited for three profiles.
- (6) Von Mises is the worst model in terms of accuracy since it cannot model the anisotropy. Furthermore, Yld89_S predicts R -values not accurately compared to other criteria, justifying the high MAPE by about 35% like the Von Mises yield function.
- (7) It can be inferred that yield stress-based calibrated criteria such as Yld89_S and Hill48_S produce more accurate results for “near the bend” profile, while R -value calibrated criteria such as Hill48_R and Yld89_R are more accurate for “on the bend” profile.

Author contribution Saeid Hajiahmadi: data curation, methodology, investigation, experiments, writing of original draft, validation, software, and visualization; Hassan Moslemi Naeini: project administration, writing including review and editing, conceptualization, and supervision; Hossein Talebi-Ghadikolaee: writing including review and editing, validation, methodology, conceptualization, and supervision; Rasoul Safdarian: writing including review and editing, validation, and supervision; Ali Zeinolabedin-Beygi: investigation, experiments, software, and writing of original draft. All the authors read and approved the final manuscript.

Funding The authors declare that no funds, grants, or other support were received during the preparation of this manuscript.

Declarations

Competing interests The authors declare no competing interests.

References

- Talebi-Ghadikolaee H et al (2023) Experimental-numerical analysis of ductile damage modeling of aluminum alloy using a hybrid approach: ductile fracture criteria and adaptive neural-fuzzy system (ANFIS). *Int J Model Simul* 43(5):736–751
- Deilami Azodi H et al (2023) Integral hydro-bulge forming of spherical vessels: a numerical and experimental study. *Iran J Mater Form* 10(2):4–11
- Talebi-Ghadikolaee H, Barzegari MM, Seddighi S (2023) Investigation of deformation mechanics and forming limit of thin-walled metallic bipolar plates. *Int J Hydrogen Energy* 48(11):4469–4491
- Safari M et al (2021) Creep age forming of fiber metal laminates: effects of process time and temperature and stacking sequence of core material. *Materials* 14(24):7881
- Rabiee AH et al (2023) Experimental investigation and modeling of fiber metal laminates hydroforming process by GWO optimized neuro-fuzzy network. *J Comput Appl Res Mech Eng (JCARME)* 12(2):193–209
- Talebi-Ghadikolaee H et al (2022) Predictive modeling of damage evolution and ductile fracture in bending process. *Mater Today Commun* 31:103543
- Elyasi M, et al (2023) The effect of aging heat treatment on the formability and microstructure of the AA6063 tube in the rotary draw bending process. *J Eng Res*. <https://doi.org/10.1016/j.jer.2023.10.017>
- Xu C-T et al (2023) A study of transverse bowing defect in cold roll-forming asymmetric corrugated channels. *Int J Adv Manuf Technol* 124(10):3567–3577
- Talebi-Ghadikolaee H et al (2020) Ductile fracture prediction of AA6061-T6 in roll forming process. *Mech Mater* 148:103498
- Hajiahmadi S et al (2023) Effect of anisotropy on spring-back of pre-punched profiles in cold roll forming process: an experimental and numerical investigation. *Int J Adv Manuf Technol* 129(9):3965–3978
- Badparva H et al (2023) Deformation length in flexible roll forming. *Int J Adv Manuf Technol* 125(3–4):1229–1238
- Safdarian R, Naeini HM (2015) The effects of forming parameters on the cold roll forming of channel section. *Thin-Walled Struct* 92:130–136
- Tajik Y et al (2018) A strategy to reduce the twist defect in roll-formed asymmetrical-channel sections. *Thin-Walled Struct* 130:395–404
- Talebi-Ghadikolaee H et al (2020) Modeling of ductile damage evolution in roll forming of U-channel sections. *J Mater Process Technol* 283:116690
- Sumikawa S, Ishiwatari A, Hiramoto J (2017) Improvement of springback prediction accuracy by considering nonlinear elastoplastic behavior after stress reversal. *J Mater Process Technol* 241:46–53
- Kim H et al (2013) Nonlinear elastic behaviors of low and high strength steels in unloading and reloading. *Mater Sci Eng, A* 562:161–171
- Chatti S, Hermi N (2011) The effect of non-linear recovery on springback prediction. *Comput Struct* 89(13):1367–1377
- Yoshida F, Uemori T, Fujiwara K (2002) Elastic–plastic behavior of steel sheets under in-plane cyclic tension–compression at large strain. *Int J Plast* 18(5–6):633–659
- Sun L, Wagoner RH (2011) Complex unloading behavior: nature of the deformation and its consistent constitutive representation. *Int J Plast* 27(7):1126–1144
- Chatti S (2013) Modeling of the elastic modulus evolution in unloading-reloading stages. *Int J Mater Form* 6(1):93–101
- Yoshida F, Amaishi T (2020) Model for description of non-linear unloading-reloading stress-strain response with special reference to plastic-strain dependent chord modulus. *Int J Plast* 130:102708
- Toros S, Polat A, Ozturk F (2012) Formability and springback characterization of TRIP800 advanced high strength steel. *Mater Des* 41:298–305
- Lin J et al (2020) Effect of constitutive model on springback prediction of MP980 and AA6022-T4. *Int J Mater Form* 13(1):1–13
- Lee J-Y et al (2012) An application of homogeneous anisotropic hardening to springback prediction in pre-strained U-draw/bending. *Int J Solids Struct* 49(25):3562–3572
- Seo KY, Kim JH, Lee HS, Kim JH, Kim BM (2017) Effect of constitutive equations on springback prediction accuracy in the TRIP1180 cold stamping. *Met* 8(1):18
- Liu X-L et al (2020) Experimental and numerical prediction and comprehensive compensation of springback in cold roll forming of UHSS. *Int J Adv Manuf Technol* 111(3):657–671
- Naofal J, Naeini HM, Mazdak S (2019) Effects of hardening model and variation of elastic modulus on springback prediction in roll forming. *Metals* 9(9):1005
- Bidabadi BS et al (2016) Experimental study of bowing defects in pre-notched channel section products in the cold roll forming process. *Int J Adv Manuf Technol* 87(1):997–1011
- Shirani Bidabadi B et al (2015) Experimental investigation of the ovality of holes on pre-notched channel products in the cold roll forming process. *J Mater Process Technol* 225:213–220
- Nasrollahi V, Arezoo B (2012) Prediction of springback in sheet metal components with holes on the bending area, using experiments, finite element and neural networks. *Mater Design* 1980–2015(36):331–336
- Nikhare CP, Kotkunde N, Singh SK (2021) Effect of material discontinuity on springback in sheet metal bending. *Adv Mater Process Technol* 8(sup3):1800–1819
- Liu X et al (2017) Investigation of forming parameters on springback for ultra high strength steel considering Young's modulus variation in cold roll forming. *J Manuf Process* 29:289–297
- Jiao-Jiao C et al (2020) A novel approach to springback control of high-strength steel in cold roll forming. *Int J Adv Manuf Technol* 107:1793–804
- Badr OM et al (2017) Applying a new constitutive model to analyse the springback behaviour of titanium in bending and roll forming. *Int J Mech Sci* 128:389–400
- Zhao K et al (2016) Identification of post-necking stress–strain curve for sheet metals by inverse method. *Mech Mater* 92:107–118
- Kruglov AA, Enikeev FU, Lutfullin RY (2002) Superplastic forming of a spherical shell out a welded envelope. *Mater Sci Eng, A* 323(1):416–426
- Hill R (1948) A theory of the yielding and plastic flow of anisotropic metals. *Proc Roy Soc Lond. Ser A. Math Phys Sci* 193(1033):281–297
- Barlat F, Lian K (1989) Plastic behavior and stretchability of sheet metals. Part I: a yield function for orthotropic sheets under plane stress conditions. *Int J Plast* 5(1):51–66
- Hosford WF (1970) On the crystallographic basis of yield criteria. *Textures Microst* 26(1):479–93

40. Barlat F et al (2003) Plane stress yield function for aluminum alloy sheets—part I: theory. *Int J Plast* 19(9):1297–1319
41. Waltz RA et al (2006) An interior algorithm for nonlinear optimization that combines line search and trust region steps. *Math Program* 107(3):391–408
42. Byrd RH, Hribar ME, Nocedal J (1999) An interior point algorithm for large-scale nonlinear programming. *SIAM J Optim* 9(4):877–900
43. Hellborg S (2007) Finite Element Simulation of Roll Forming. Dissertation, Institute of Technology Linköping University
44. ShiraniBidabadi B et al (2022) Investigation of over-bending defect in the cold roll forming of U-channel section using experimental and numerical methods. *Proc Inst Mech Eng, Part B: J Eng Manuf* 236(10):1380–1392
45. Poursafar A et al (2022) Experimental and mathematical analysis on spring-back and bowing defects in cold roll forming process. *IntJ Interact Design Manuf (IJIDeM)* 16(2):531–543
46. Paralikas J, Salonitis K, Chryssolouris G (2010) Optimization of roll forming process parameters—a semi-empirical approach. *Int J Adv Manuf Technol* 47:1041–1052
47. Bui QV, Ponthot JP (2008) Numerical simulation of cold roll-forming processes. *J Mater Process Technol* 202(1):275–282
48. Sherkatghanad E et al (2021) Modeling and predicting the important properties of the PVC/glass fiber composite laminates in the production process by the TLBO-ANFIS approach. *Iran J Mater Form* 8(4):63–75
49. Bowerman B et al (2005) *Forecasting, Time Series, and Regression: An Applied Approach*. Thomson Brooks/Cole, California

Publisher's Note Springer Nature remains neutral with regard to jurisdictional claims in published maps and institutional affiliations.

Springer Nature or its licensor (e.g. a society or other partner) holds exclusive rights to this article under a publishing agreement with the author(s) or other rightsholder(s); author self-archiving of the accepted manuscript version of this article is solely governed by the terms of such publishing agreement and applicable law.